Quest for magnons in ultrathin nickel films

H. Ibach* and C. M. Schneider
Peter Grünberg Institut (PGI-6), Forschungszentrum Jülich, 52425 Jülich, Germany
and Jülich Aachen Research Alliance, Germany

(Received 11 June 2018; revised manuscript received 22 June 2018; published 10 July 2018)

High-momentum spin waves (magnons) in ultrathin films of cobalt and iron have been explored thoroughly using inelastic scattering of low-energy electrons. The search for magnons in ultrathin nickel films failed, however, although high-energy magnons do exist in bulk nickel. The failure might be due to the weak coupling of nickel magnons to scattering electrons. In order to increase the coupling we deposited layers of cobalt onto Ni films and successfully studied the magnons of such films. The acoustic modes show the same dispersion as pure Co films, which is consistent with the nearly identical stiffness of bulk magnons in nickel and cobalt. Standing magnons in Ni films covered with Co are strongly damped at the Ni/Cu(100) interface when their total wave vector exceeds about $3\,\mathrm{nm}^{-1}$.

DOI: 10.1103/PhysRevB.98.014413

I. INTRODUCTION

Despite their delocalized ("itinerant") nature, $3d$ electrons of iron, cobalt, and nickel sustain high-momentum spin waves (magnons). Early experimental evidence for magnons in bulk material stems from inelastic neutron scattering [1–3]. Already in 1967 Mills proposed to employ inelastic scattering of low-energy electrons to investigate high-momentum magnons at surfaces and in thin films [4]. It took, however, several decades to overcome the technical difficulties involved in high-resolution/high-sensitivity inelastic electron scattering until the first successful study on thin-film magnons was performed [5]. In the years to follow numerous studies were published on ultrathin films of fcc cobalt [6,7], iron [8–11], and FeCo films [12,13]. Because of the limited energy resolution, the experimental data base was initially confined to wave vectors above $q_\parallel \approx 3\,\mathrm{nm}^{-1}$. In that range, the lifetime of magnons is extremely short (<100 fs) [14,15]. Consequently, the N eigenmodes of an N-layer film overlap to become a broad feature, which cannot be disentangled into individual modes. Partly because of this problem, many early studies focused on single-atom-layer films which sustain only a single magnon mode (see, e.g., [15,16]). With further improvements of dedicated electron spectrometers [17,18], experimental studies could be extended to magnons with wave vectors between $q_\parallel = 1\,\mathrm{nm}^{-1}$ and $q_\parallel = 3\,\mathrm{nm}^{-1}$. In that range, the lifetime of magnons is longer so that in addition to the acoustic mode one or two of the standing modes of a film become distinct features in energy-loss spectra [6,19–21]. These standing modes are likewise characterized by a wave vector $q_\parallel$ and additionally by one to $N-1$ nodes inside the film. The energy of the first standing mode with a single node inside the film roughly scales inversely proportional to the square of the thickness of the layer [6,19].

Because of the small damping of modes with wave vectors below $3\,\mathrm{nm}^{-1}$, the eigenmodes of films are adequately and surprisingly well described in the Heisenberg model of localized spins. Even shapes of spectra can be modeled when the finite penetration depth of low-energy electrons and the finite lifetime of magnons are properly taken into account [22].

According to neutron scattering the exchange stiffness of bulk magnons of nickel and fcc cobalt is nearly the same ($3.74\,\mathrm{meV\,nm}^2$, $3.84\,\mathrm{meV\,nm}^2$, respectively) [2,3,23]. Thin films of Ni grow epitaxially on Cu(100) [24]. The Curie temperature rises with the film thickness and lies above 300 K beyond a film thickness of about four atom layers [25,26]. The magnetization undergoes a gradual reorientation from parallel to perpendicular around a film thickness of eight atom layers [25–27].

In view of these results one would expect to see a magnon response also in inelastic electron scattering from nickel films. Rajeswari has made an attempt to find magnons in ten-atom-layer epitaxial Ni films on Cu(100) [28] but, however, failed to see any in the investigated range of wave vectors between $4\,\mathrm{nm}^{-1}$ and $8\,\mathrm{nm}^{-1}$. In a further experiment of Rajeswari *et al.* [29], a film of eight fcc Co layers deposited on Cu(100) was covered by up to four layers of Ni. The only noticeable effect of the Ni film on the magnon response (at $q_\parallel = 7\,\mathrm{nm}^{-1}$) was a reduction of the intensity of the cobalt magnon signal. The intensity decays exponentially with the thickness of the Ni film and is quantitatively described by the mean free path of electrons in nickel [30]. Furthermore, in the course of this study we have searched for magnons in Ni films in the low-wave-vector range $q_\parallel < 3\,\mathrm{nm}^{-1}$ that is now accessible, however in vain.

The negative result of all these experiments suggests that magnons in ultrathin Ni films are either drastically damped or their cross section for inelastic scattering is much smaller than for cobalt and iron films. A large damping concomitant with a reduced magnon energy is predicted by theory for an epitaxial single atom layer of Ni on Cu(100) [31]. It is not known, however, to what extent magnons in thicker Ni layers

*h.ibach@fz-juelich.de

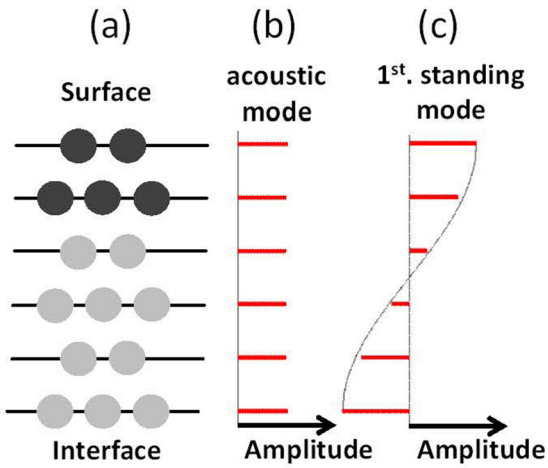

FIG. 1. Classical precession amplitudes of the two lowest eigenmodes of a six-layer film (a) with homogenous exchange coupling shown as red bars (see text for details).

are also affected. However, one would expect the damping to be primarily an interface effect and thus to gradually disappear for thicker films.

A small cross section for inelastic electron scattering from Ni films is plausible as the cross section should scale with the square of the magnetic moment [32]. Magnetic moments of seven-atom-layer fcc epitaxial films of Co and Ni on Cu(100) surfaces have been calculated by Hjortstam *et al.* [33]. For the center layer they find 0.59 μ_B and 1.63 μ_B for Ni and Co, respectively. These numbers are in agreement with polarized neutron reflection experiments [34]. The intensity of magnons in the spectra of Ni films should therefore be one-eighth of that of Co magnons. The analysis of the spectra of Ni films by Rajeswari [28] suggests that the cross section must be even smaller.

II. CONCEPT OF THE EXPERIMENT

To explore the role of the cross section we study electron energy-loss spectra of Ni films covered by a few atomic layers of cobalt with the idea that cobalt would provide the coupling to the scattering electrons, whereas the spectra should reflect the exchange coupling between the Co atoms as well as between the Ni atoms below. Since bulk magnons of cobalt and nickel have a similar stiffness, one expects the magnon modes of the composite film to be reasonably well represented by the Heisenberg model with homogeneous exchange coupling constants. Figure 1 illustrates the classical precession amplitudes of the two lowest eigenmodes of a six-layer film [Fig. 1(a)] with homogenous exchange coupling. The wave vector parallel to the surface is $q_\parallel = 1.8\,\mathrm{nm}^{-1}$. For higher wave vectors near the boundary of the Brillouin zone, the two modes mix to becomes modes localized at the surface and interface, respectively. In the context of this paper we are interested in the low-wave-vector range, since only in that range magnons are well-defined excitations in itinerant magnets.

The lowest energy mode is the acoustic mode [Fig. 1(b)]. Disregarding small anisotropy effects of the order of 0.1 meV, its energy becomes zero at $q_\parallel = 0$, as at $q_\parallel = 0$ the mode

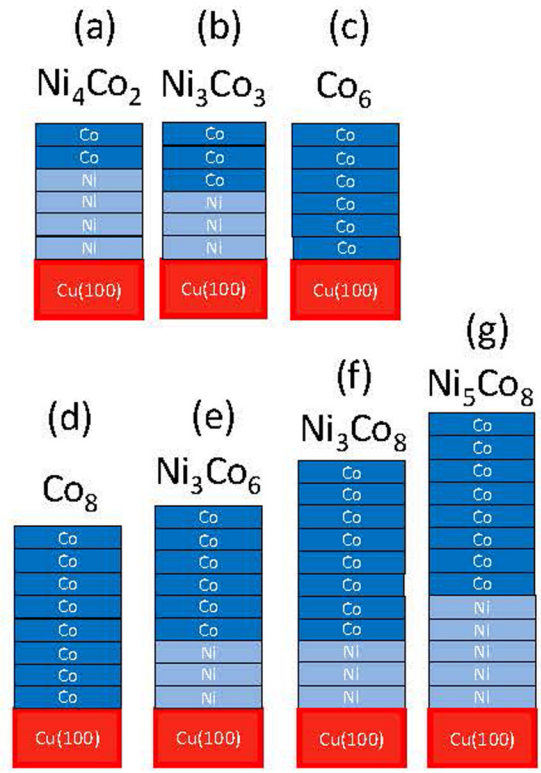

FIG. 2. Illustration of the investigated layer systems.

corresponds to a uniform magnetization. The next mode higher up in energy is the first standing with one node in the precession amplitude [Fig. 1(c)]. If the center of the film is a mirror plane, modes are either even or odd with respect to the center plane and the node is therefore in the center plane. Higher-energy standing modes with two or more nodes are not observed on Cu(100) because of their large damping. They are found, however, in epitaxial cobalt films on W(110) [19].

In a first set of experiments we have fabricated two types of six-atom-layer films on Cu(100), one with four atomic layers of nickel covered by two layers of cobalt [denoted as Ni_4Co_2, Fig. 2(a)]. A second one comprised of three nickel layers topped by three layers of cobalt [Ni_3Co_3, Fig. 2(b)]. We find the acoustic mode of the Ni_4Co_2 and Ni_3Co_3 films to possess the same dispersion as a six-atom-layer cobalt film [Fig. 2(c)]. Since two- and three-atom-layer Co films on Cu(100) exhibit no magnons and magnons with a reduced stiffness, respectively, we conclude that the Ni layers do participate in the magnon spectrum and that the exchange interaction between the Ni atoms of the film is comparable to the exchange between cobalt atoms. This is one main result of this paper.

Surprisingly, however, the characteristic standing mode of a six-layer film [Fig. 1(c)] is not found in Ni_3Co_3 and Ni_4Co_2. In order to explore further the role of Ni layers under the Co film we have deposited thicker Co layers (Co_6 and Co_8) on Cu(100)/Ni_3 and Cu(100)/Ni_5 substrates [Figs. 2(e)–2(g)]. Now intense signals of the first standing mode of the Ni_3Co_6 and Ni_3Co_8 films are found with a dispersion curve characteristic for standing waves. The dispersion curves fall below the dispersion curves of Co_6 and Co_8 deposited directly

on Cu(100) [Figs. 2(c) and 2(d)]. An analysis of the standing-wave dispersion of the systems depicted in Figs. 2(e)–2(g) based on the Heisenberg model shows that the dispersion is approximately the same as for pure cobalt films with an effective film thickness increased by two atom layers. We therefore conclude that about two Ni layers adjacent to the cobalt layers participate in the standing mode excitation. The finite penetration depth of magnons into the Ni film as well as their absence in spectra of Ni_4Co_2 [Fig. 2(a)] and Ni_3Co_3 [Fig. 2(b)] is attributed to a strong, wave-vector-dependent damping of the standing magnons at the Ni/Cu interface. The reduced magnetic moment of Ni at the Cu interface [35] may also contribute.

The paper is organized as follows. The next section describes experimental technique and sample preparation. Since the quality of the spectra depends critically on the quality of the deposited films, the section discusses some details of the preparation and characterization of the films. Section IV shows results for Ni_4Co_2 and Ni_3Co_3 films [Figs. 2(a) and 2(b)]. The results for thicker Co layers deposited on Ni_3 films and Ni_5 films [Ni_3Co_6,Ni_3Co_8, and Ni_5Co_8, Figs. 2(e)–2(g)] are presented in Sec. V. Section VI analyzes the dispersion of the acoustic and standing modes of the films with the help of the Heisenberg model and compares the results to theory. Section VII provides a summary.

III. EXPERIMENT

The electron-energy-loss spectrometer used in our experiments is of the type described in [18,36], equipped with a new, more compact electron emission system. The spectrometer is operated at <3 meV and ~4 meV resolution, depending on the sharpness of the magnon features of interest. The electron impact energy was $E_0 = 2.25$ eV. The wave vector parallel to the surface $q_\parallel$ is determined by making use of wave-vector conservation, which for an energy loss is

$$q_{||} = k^{(\mathrm{f})} \sin(\theta^{(\mathrm{f})}) - k^{(\mathrm{i})} \sin(\theta^{(\mathrm{i})}). \quad (1)$$

Here, $k^{(\mathrm{i})}$ and $k^{(\mathrm{f})}$ are the moduli of k vectors of the incident and scattered electron, respectively, and $q^{(i)}$ and $q^{(\mathrm{f})}$ are the angles with respect to the normal of the surface (Fig. 3). The desired wave vector of the magnon parallel to the surface is chosen by rotation of the sample around the axis vertical to the scattering plane spanned by the vectors $\boldsymbol{k}^{(\mathrm{i})}$ and $\boldsymbol{k}^{(\mathrm{f})}$.

Spectra are recorded at fixed rotation angle. Since the electron impact energy is relatively low, the true wave vector varies slightly with the magnitude of the energy loss. For example, for $E_0 = 2.25$ eV, a nominal wave vector of $q_\parallel = 2\,\mathrm{nm}^{-1}$, and an energy loss of 15 meV the true wave vector is $1.97\,\mathrm{nm}^{-1}$.

The films are prepared by e-beam-assisted evaporation from Ni and Co rods onto Cu(100) substrates at room temperature. The film thicknesses are calibrated vs the ion current of the evaporator via the oscillations in the intensity of reflected 3-keV electrons at grazing incidence ("MEED oscillations") [7,19,22]. A quartz microbalance calibrated vs the intensity oscillations is also employed for in-between checks.

The lateral order of the films is probed by low-energy-electron diffraction (LEED). As an example, Fig. 4 shows the LEED pattern of a six-layer film of the type Ni_3Co_3.

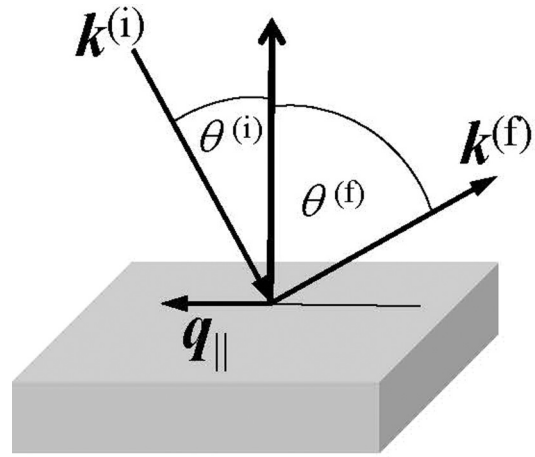

FIG. 3. Illustration of the scattering geometry.

A good measure of disorder is the elastic diffuse scattering. In the ideal case of perfect order, the intensity outside the diffracted beams is entirely due to inelastic processes, predominantly due to phonon scattering. When measured with an instrument of high energy resolution enabling the separation of the true elastic scattering from phonon scattering, the intensity outside the diffracted beam is proportional to the disorder in the film; it depends, however, also on the type of disorder. For epitaxial films with sufficiently low contamination levels the disorder is mainly in the form of atomic steps.

Figure 5 displays an example of the elastic intensity as function of the lateral wave-vector transfer $q_\parallel$ for two different films, an eight-layer Co film and a Ni_4Co_4 film (red open squares and blue circles, respectively). The films are annealed after deposition to temperatures up to 450 K for 15 min. At this temperature the surface diffusion of Co atoms across steps is large enough to initiate smoothening of the surface and thereby a reduction of the density of surface steps. As shown in [21], this procedure reduces the density of surface steps while still no copper creeps to the surface.

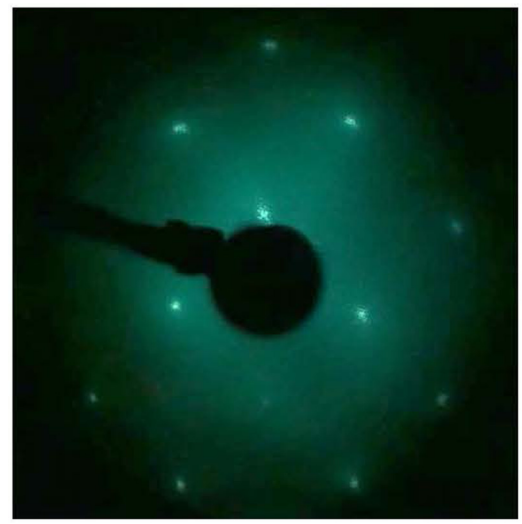

FIG. 4. LEED pattern at 167 eV of a Ni_3Co_3 film (total of six layers).

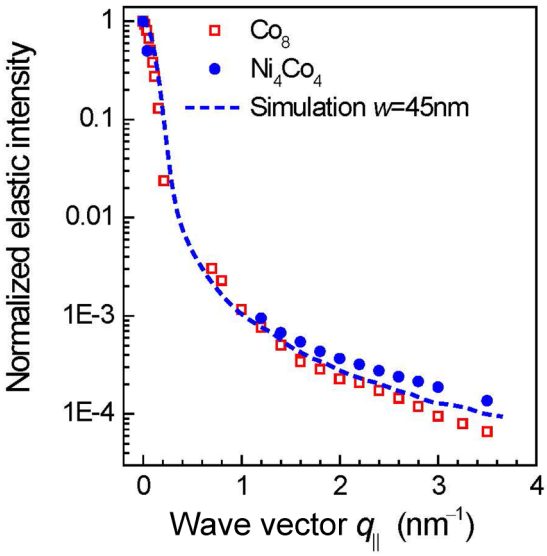

FIG. 5. Elastic intensity as function of the wave-vector transfer for an eight-layer Co film Co_8 and a Ni_4Co_4 film is shown as red open squares and blue solid circles, respectively. The blue dashed line is a simulation assuming that the diffuse scattering is caused by a random array of steps with a mean terrace width $w = 45$ nm.

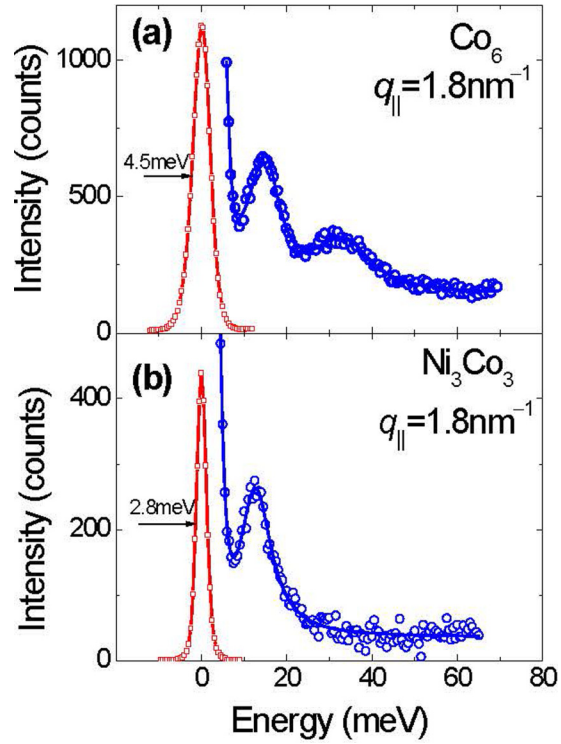

FIG. 6. Magnon spectra for Co_6 and Ni_3Co_3 films deposited on Cu(100). The spectra are corrected for the Bose occupation number. Data accumulation time is 6 s/channel. The Co_6 spectrum is obtained with less resolution to boost the intensity of the intrinsically broader standing mode.

The intensity plotted in Fig. 5 is normalized to the specular beam ($q_{||} = 0\,\mathrm{nm}^{-1}$). Near specular direction the intensity is measured by using the channeltron electron multiplier as a Faraday cup connected to a pico-amperemeter; farther off the specular beam the intensity is measured as the electron count rate. The blue dashed line in Fig. 5 is the result of a calculation of the elastic surface scattering from a (100) surface with a random distribution of up and down steps (see [21] for details). The assumed mean terrace width is 180 atom lengths (equivalent to $w \approx 45$ nm). The theoretical result approximately matches the experimental data in the entire momentum range. The results displayed in Fig. 5 demonstrate that the Ni_4Co_4 film is nearly as well ordered as the eight-layer Co film.

IV. RESULTS FOR Ni_3Co_3 AND Ni_4Co_2

Characteristic energy-loss spectra for two different six-layer films, Co_6 and Ni_3Co_3, are displayed in Fig. 6. The impact energy is 2.25 eV. The nominal wave vector is $q_{||} = 1.8\,\mathrm{nm}^{-1}$, oriented along the [110]($\bar{\Gamma}$ $\bar{X}$) direction. The open red squares show the elastic diffuse lines with the FWHM marking the resolution. The intensities of energy losses $\hbar\omega$ scale with $n(\hbar\omega,T)+1$, where n is the Bose occupation number. The spectral density is therefore recovered from the data by dividing the energy-loss spectrum by $n(\hbar\omega,T)+1$ (blue circles in Fig. 6).

The solid blue lines are fits by a Gaussian for the tail of the elastic peak, Lorentzians for the magnons, and a constant background. The Co_6 film [Fig. 6(a)] shows the acoustic mode at 13 meV and the first standing mode at 33 meV [6,21]. The standing mode is missing in spectrum (6b), which is for the Ni_3Co_3 film, while the acoustic mode remains at 13 meV and is as sharp and intense as for pure Co. The same result is obtained for a four-layer Ni film covered by two atom layers of Co (Fig. 7).

Three-atom-layer-thick Ni films on Cu(100) without Co layers on top have a Curie temperature of about 180 K [25]. To ensure that the absence of the standing mode in the Ni_3Co_3 and Ni_4Co_2 systems is not related to a loss of long-range order due to a low Curie temperature of the films, we have studied spectra at lower temperatures. Figure 7 compares the result for a Ni_4Co_2 film at 300 K and 90 K. When corrected for the Bose occupation number, the magnon spectra of the Ni_4Co_2 film at 300 K and 90 K are identical.

Figure 8 shows the dispersion of the acoustic modes for the Ni_3Co_3,Ni_4Co_2,Co_6, and Co_3 films as red squares, magenta diamonds, olive triangles, and blue inverted triangles, respectively. Within the error margins, dispersion curves for Ni_3Co_3,Ni_4Co_2, and Co_6 are identical, whereas the data for the Co_3 layer fall below the data of the six-layer films.

The Curie temperature of a three-layer cobalt film is still well above room temperature (600 K [37]). The reduced magnon energies are therefore not to be attributed to a low Curie temperature but rather to the larger influence of surface and interface in three-layer films. A two-layer cobalt film on Cu(100) does not sustain magnons at room temperature, since then the Curie temperature is only about 300 K [37]. The Ni_4Co_2 film possesses well-defined acoustic magnons therefore only because of the Ni layers underneath.

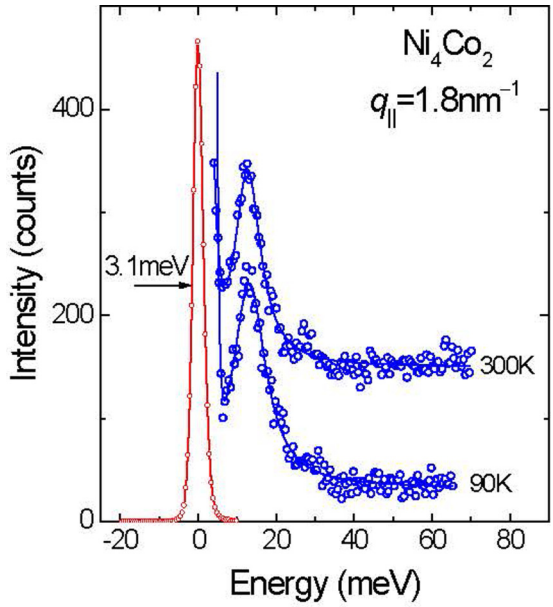

FIG. 7. Magnon spectra of a Ni_4Co_2 film corrected for the Bose occupation number at 300 K and 90 K. The acoustic mode is at the same energy at both temperatures.

The dispersion of acoustic magnons for small wave vectors is described by a quadratic dependence of the magnon energy $\hbar\omega$ on the wave vector $q_\parallel$:

$$\hbar\omega = Dq_\parallel^2, \tag{2}$$

in which D is called the exchange stiffness of magnons. Equation (2) neglects small Dzyaloshinsky-Moriya [38,39] effects as well as anisotropy effects and higher-order terms. The dashed line in Fig. 8 marks the $q_\parallel^2$ dependence for the acoustic modes in Ni_4Co_2, Ni_3Co_3, and Co_6 films. The stiffness for these three types of films is 3.7 meVnm^2. The exchange stiffness for the three-layer Co film (blue down triangles in Fig. 8) is about 15% lower (3.2 meVnm^2). Since the amplitude of the acoustic magnon is (at least roughly) homogeneous across the film, the identical stiffness for Co_6, Ni_3Co_3, and Ni_4Co_2 films entails that the Ni layers have about the same exchange coupling as the cobalt layers. Furthermore, the stiffness of magnons in the film is about equal to the stiffness of bulk magnons in Ni and fcc Co (3.74 meV nm^2, 3.84 meV nm^2 [23], respectively). Finally, the damping of magnons of Ni_3Co_3 and Ni_4Co_2 films with small wave vectors parallel to the surface is about as small as it is for Co films (see Fig. 6).

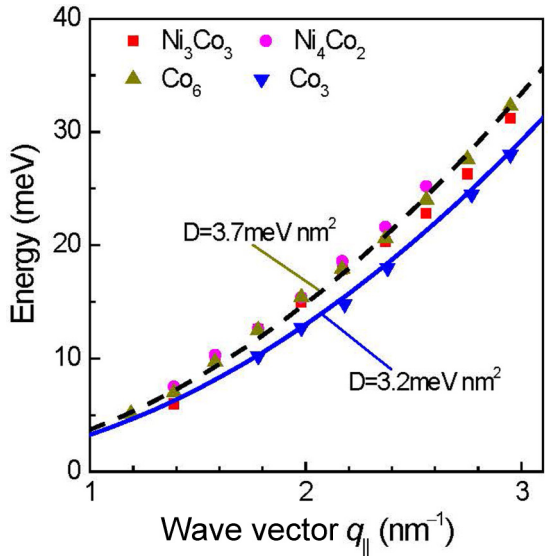

FIG. 8. Dispersion data of the acoustic mode of four different films, Ni_3Co_3, Ni_4Co_2, Co_6, and Co_3, are shown as red squares, magenta diamonds, olive up triangles, and blue down triangles. The dashed line is a common parabola fit to Ni_3Co_3, Ni_4Co_2, and Co_6 according to Eq. (2), the solid line the same fit to the three-layer Co film.

Thus, when considering merely the acoustic mode one is lead to the conclusion that the exchange coupling in nickel and cobalt films is alike not only in bulk material but also in thin films. The absence of a magnon signal in the energy-loss spectra of pure nickel films is therefore to be attributed entirely to a small cross section for inelastic electron scattering in the case of nickel.

What remains a mystery at this point is the complete absence of a spectral signature of standing magnons in Ni_3Co_3 and Ni_4Co_2 films (Figs. 6 and 7). In order to learn more about this mystery, three- and five-layer nickel films covered with thicker cobalt films are studied in the next section.

V. RESULTS FOR Ni_3Co_6, Ni_3Co_8, AND Ni_5Co_8

Figure 9 shows three spectra for an eight-layer cobalt film, (a) deposited directly on Cu(100) and (b, c) deposited on top of a three- and five-layer nickel film on Cu(100), respectively. The nominal wave vector is $q_\parallel = 1.8\,\mathrm{nm}^{-1}$. Now, with the thicker cobalt films standing modes show up. Compared to the pure cobalt film the modes are downshifted in energy (see dashed line), which is qualitatively consistent with the larger total number of layers, as the energy of the standing wave is lower the larger the number of atom layers in the film. Surprisingly, however, the magnitude of the downshift is identical for the Ni_3 and Ni_5 underlay. Dispersion curves of the acoustic mode and the lowest standing mode of Co_6 and Ni_3Co_6 films and of Co_8 and Ni_3Co_8 films are shown in Figs. 10(a) and 10(b), respectively. The range of wave vectors is smaller than for thinner films for the following reason: A lower limit is set by the increasing elastic diffuse intensity at small $q_\parallel$ (see Fig. 5). The upper limit is caused by the merging energies of standing and acoustic modes. Within that window, the dispersion of the acoustic mode is identical for all films. The downshift of the standing mode by the Ni underlay concerns the entire range in which the standing mode could be probed. The downshift is larger for the six-layer Co film [Fig. 10(a)]. The lines in Figs. 10(a) and 10(b) are calculated in a nearest-neighbor Heisenberg model, which is considered in the next section.

VI. DISCUSSION

The downshift of the standing waves with the Ni underlay is qualitatively consistent with a larger number of layers participating in the standing wave motion. The fact that the downshift does not continue when the Ni underlay is thicker

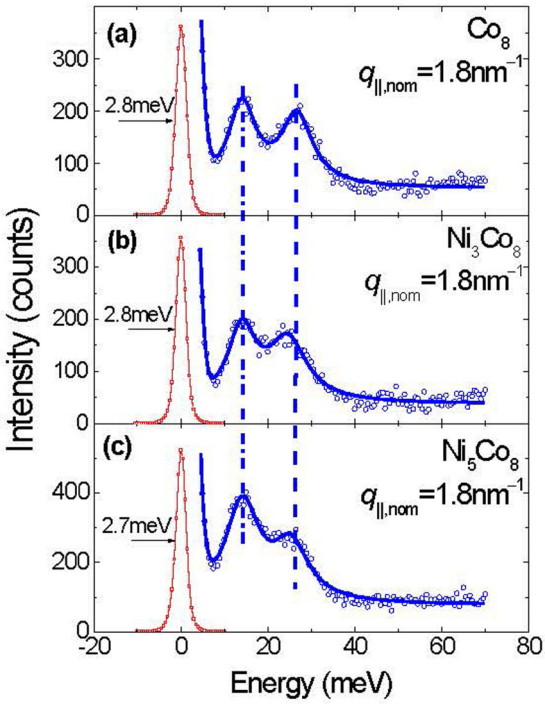

FIG. 9. Sample spectra of Co_8, Ni_3Co_8, and Ni_5Co_8 films for a wave vector of $q_{\parallel} = 1.8\,\mathrm{nm}^{-1}$. The acoustic mode has the same energy in all three films (dash-dotted line) are shown in (a), (b), and (c), respectively. All spectra show a standing mode. In films with a nickel underlay (b), (c) the energy is downshifted (dashed line).

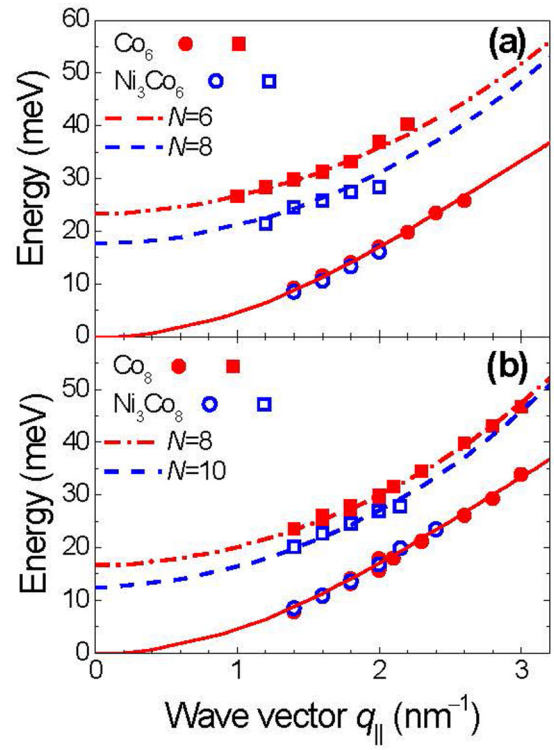

FIG. 10. (a) Dispersion data for the acoustic and standing modes of Co_6 (red solid circles and squares, respectively) and Ni_3Co_6 (open blue circles and squares, respectively). (b) Data for the acoustic and standing modes of Co_8 (red solid circles and squares, respectively) and Ni_3Co_8 (open blue circles and squares, respectively). The lines are calculated in a Heisenberg model (see text for discussion).

[Fig. 9(c)] seems to indicate that only Ni layers adjacent to Co participate. A full understanding of this effect requires theory that takes the interaction of magnons with spin-flip single-electron excitations (Stoner excitations) into account, which is far beyond the scope of this experimental study. In order to describe the dispersion curves in Fig. 10 and to obtain at least a hint as to the reason for the absence of standing waves in Figs. 6 and 7 we resort to the Heisenberg model. The model neglects the role of Stoner excitations and thereby Landau damping all together and is therefore not to be used to describe higher-wave-vector magnon excitations (for a critical discussion see [40]). It is, however, suitable to describe the dispersion of magnons in the low-wave-vector range [22].

Earlier studies on cobalt films have found exchange coupling constants to depend on the position of the layers relative to the surface and interface (see, e.g., [41,42]). Such calculations are not available for the complex NiCo films studied here. For a heuristic description of the dispersion curve it suffices to consider a simple nearest-neighbor Heisenberg model.

For a (100)-oriented N-layer fcc film along the $\overline{\Gamma X}[1\bar{1}0]$ direction the secular equation is

$$\begin{pmatrix} \alpha_1 - E & \beta_1 & 0 & & 0 \\ \beta_1 & \alpha_2 - E & \beta_2 & & 0 \\ 0 & & & & \\ 0 & & & \beta_{N-1} & \alpha_N - E \end{pmatrix} \begin{pmatrix} A_1 \\ A_2 \\ \\ A_N \end{pmatrix} = 0, \tag{3}$$

in which E is the reduced energy

$$E = \hbar\omega/8J. \tag{4}$$

The coefficients α_n and β_n are

$$\begin{aligned} \alpha_1 &= 0.5(1 - \cos q_{||}a) + C_{12}, \beta_1 = -C_{12}\cos q_{||}a/2\alpha_2 \\ &= 0.5(1 - \cos q_{||}a) + C_{23} + C_{12}, \\ \alpha_{n>2,\neq N} &= 0.5(1 - \cos q_{||}a) + C_{n,n+1} + C_{n,n-1}\,\beta_{n>1} \\ &= -C_{n,n+1}\cos q_{||}a/2\alpha_N \\ &= 0.5(1 - \cos q_{||}a) + C_{N,N-1}. \end{aligned} \tag{5}$$

Here, a is the surface lattice constant of the film ($a = 0.256$ nm). The coefficients $C_{n,n+1}$ permit the interlayer exchange coupling between layer n and layer $n+1$ to be different from the intralayer coupling. We assume all the intralayer and interlayer exchange coupling constants to be equal ($J = 19$ meV) with the exception of the interlayer coupling between the Nth Co layer next to the interface to copper and the penultimate Co layer. This interlayer coupling is set to $J_{N,N-1} = 3.2$ meV. Despite its simplicity, the model describes the dispersion of the acoustic and standing modes of the pure cobalt films surprisingly well, independent of the thickness of the film [dash-dotted and solid lines in Figs. 10(a) and 10(b)].

We remark in passing that the choice of parameters is not unique. For example, one could split the softening of the

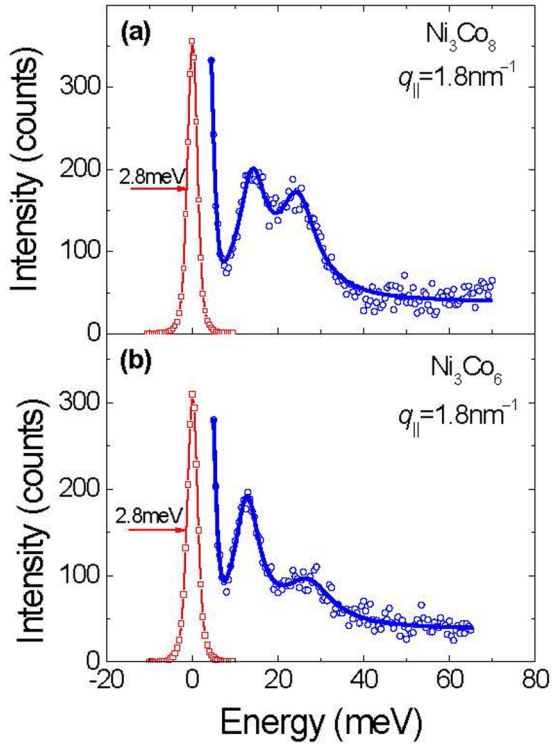

FIG. 11. Comparison of spectra at $q_{\parallel} = 1.8\ \mathrm{nm}^{-1}$ for the Ni_3Co_8 and Ni_3Co_6 films. The standing wave for the latter film is significantly more damped.

exchange coupling to occur at both the interface and at the surface and would obtain the same set of dispersion curves.

To probe the hypothesis that only a few layers of the underlying Ni films contribute to the dispersion, we calculate the dispersion curves with the same parameters for $N = 8$ and $N = 10$ layers, thereby assuming that the two Ni layers adjacent to the Co layers are exchange coupled as if they were Co layers. The resulting dispersion curves match the experimental data for Ni_3Co_6 and Ni_3Co_8 [dashed blue lines in Figs. 10(a) and 10(b)].

A plausible reason as to why only about two layers should contribute could be that standing magnons are damped inside the Ni film. Strong damping could also be the reason for the absence of standing waves in spectra of Ni_3Co_3 and Ni_4Co_2 films. If so, then the damping should be larger the thinner the cobalt layer on top of a nickel layer. Figure 11 compares spectra of Ni_3Co_8 and Ni_3Co_6 films [see Figs. 2(e) and 2(f)] obtained at $q_{\parallel} = 1.8\ \mathrm{nm}^{-1}$. Clearly, the damping is much stronger for Ni_3Co_6, which has the thinner cobalt layer on top [Fig. 11(b)].

At this point it is useful to consider that a standing mode of a film (Fig. 1) is roughly equivalent to a mode with a wave-vector component perpendicular to the film plane. This perpendicular component is approximately

$$q_{\perp} = \frac{\pi}{Nd}, \tag{6}$$

in which N is the number of layers and d the interlayer distance [Fig. 1(c)]. With $d \approx 0.17$ nm [24,43], one obtains perpendicular wave vectors $q_{\perp} = 3.08\,\mathrm{nm}^{-1}$, $q_{\perp} = 2.05\,\mathrm{nm}^{-1}$, and $q_{\perp} = 1.68\ \mathrm{nm}^{-1}$ for six-, nine-, and eleven-atom-layer films. The total wave vector of the standing mode is then

$$q = (q_{\perp}^2 + q_{||}^2)^{1/2}. \tag{7}$$

For the six-, nine-, and eleven-layer films and a parallel component of the wave vector of $q_{\parallel} = 1.8\,\mathrm{nm}^{-2}$ one therefore has total wave vectors of $3.57\,\mathrm{nm}^{-2}$, $2.73\,\mathrm{nm}^{-2}$, and $2.46\,\mathrm{nm}^{-2}$, respectively. Standing waves with a total wave vector $q = 2.73\,\mathrm{nm}^{-2}$ and $q = 2.46\,\mathrm{nm}^{-2}$ are seen in the spectra of nine- and eleven-layer films (e.g., in Fig. 11), while standing waves with a total wave vector of $q = 3.57\,\mathrm{nm}^{-2}$ are not seen in spectra of six-layer films (Figs. 6 and 7). Assigning the failure to see standing modes for the Ni_3Co_3 and Ni_4Co_2 six-layer films to high damping therefore entails that a steep increase in the damping must exist somewhere between $q = 2.7\,\mathrm{nm}^{-1}$ and $3.5\,\mathrm{nm}^{-1}$.

Such a steep increase of the damping was found in a theoretical study of Buczek *et al.* [31] for acoustic modes in Ni monolayers deposited on Cu(00). The authors compared magnons in single atom layers of nickel, cobalt, and iron on Cu(100) using time-dependent density functional theory. While for Co monolayers on Cu(100) the magnon dispersion is comparable to a freestanding Co layer and the damping remains moderate, the supported Ni layer shows a drastic reduction of the magnon energy accompanied by a dramatic increase of the damping. The effect is attributed to a reduction of the exchange splitting, a smaller magnetic moment, and a larger energy width of the Stoner continuum when the Ni film is in contact with Cu(100) [31]. According to the calculations, the magnon damping in the Cu-supported Ni layer is a steep function of the wave vector $q_{\parallel}$. Beyond about $q_{\parallel} = 3\ \mathrm{nm}^{-1}$ the FWHM of the magnon response becomes larger than the peak energy (Fig. 16 in [31]) and the magnons cease to be defined excitations. While the theoretical study of Buczek *et al.* so far concerns merely the damping of the acoustic mode in a Ni monolayer, the reasoning of Buczek *et al.* makes a strong, wave-vector-dependent damping of standing modes at the interface also likely.

VII. SUMMARY

The dispersion of the acoustic mode of Ni_3Co_3 and Ni_4Co_2 layers shows that the Ni layers contribute with about the same exchange coupling as the Co layers. This is in agreement with the fact that bulk magnons in Ni and fcc Co have the about same stiffness. The failure to see magnons in nickel in previous studies is therefore attributed to a small cross section for inelastic electron/magnon scattering in nickel.

The absence of a standing wave in spectra of Ni_3Co_3 and Ni_4Co_2 films as well as the standing-wave spectra of $Ni_{3/5}Co_{5/8}$ Ni films can possibly be understood as resulting from a strong damping of standing waves at the interface to copper when the total wave vector exceeds about $3\ \mathrm{nm}^{-1}$. An extension of the theoretical study of Buczek *et al.* to thicker layers is needed to fully resolve the issue.

ACKNOWLEDGMENTS

The authors have benefitted from enlightening discussions with A. Ernst, S. Lounis, M. Dos Santos Dias, and F. Dos Santos regarding the theory of magnons. The able technical assistance of Bernd Küpper, Arnd Bremen, and Claudia Steufmehl has been instrumental to the success of this work.

[1] D. M. Paul, P. W. Mitchell, H. A. Mook, and U. Steigenberger, Phys. Rev. B **38**, 580 (1988).
[2] H. A. Mook and D. M. Paul, Phys. Rev. Lett. **54**, 227 (1985).
[3] R. N. Sinclair and B. N. Brockhouse, Phys. Rev. **120**, 1638 (1960).
[4] D. L. Mills, J. Phys. Chem. Solids **28**, 2245 (1967).
[5] R. Vollmer, M. Etzkorn, P. S. Anil Kumar, H. Ibach, and J. Kirschner, Phys. Rev. Lett. **91**, 147201 (2003).
[6] J. Rajeswari, H. Ibach, and C. M. Schneider, Phys. Rev. Lett. **112**, 127202 (2014).
[7] J. Rajeswari, H. Ibach, C. M. Schneider, A. T. Costa, D. L. R. Santos, and D. L. Mills, Phys. Rev. B **86**, 165436 (2012).
[8] K. Zakeri, Y. Zhang, T. H. Chuang, and J. Kirschner, Phys. Rev. Lett. **108**, 197205 (2012).
[9] T.-H. Chuang, K. Zakeri, A. Ernst, L. M. Sandratskii, P. Buczek, Y. Zhang, H. J. Qin, W. Adeagbo, W. Hergert, and J. Kirschner, Phys. Rev. Lett. **109**, 207201 (2012).
[10] Y. Zhang, P. Buczek, L. Sandratskii, W. X. Tang, J. Prokop, I. Tudosa, T. R. F. Peixoto, K. Zakeri, and J. Kirschner, Phys. Rev. B **81**, 094438 (2010).
[11] J. Rajeswari, H. Ibach, and C. M. Schneider, Europhys. Lett. **101**, 17003 (2013).
[12] F. Yildiz, M. Przybylski, X.-D. Ma, and J. Kirschner, Phys. Rev. B **80**, 064415 (2009).
[13] H. J. Qin, K. Zakeri, A. Ernst, T.-H. Chuang, Y. J. Chen, Y. Meng, and J. Kirschner, Phys. Rev. B **88**, 020404 (2013).
[14] Y. Zhang, T. H. Chuang, K. Zakeri, and J. Kirschner, Phys. Rev. Lett. **109**, 087203 (2012).
[15] H. J. Qin, K. Zakeri, A. Ernst, L. M. Sandratskii, P. Buczek, A. Marmodoro, T.-H. Chuang, Y. Zhang, and J. Kirschner, Nat. Commun. **6**, 6126 (2015).
[16] K. Zakeri, J. Prokop, Y. Zhang *et al.*, Surf. Sci. **630**, 311 (2014).
[17] H. Ibach, F. C. Bocquet, J. Sforzini *et al.*, Rev. Sci. Instrum. **88**, 033903 (2017).
[18] H. Ibach and J. Rajeswari, J. Electron Spectrosc. Relat. Phenom. **185**, 61 (2012).
[19] E. Michel, H. Ibach, and C. M. Schneider, Phys. Rev. B **92**, 024407 (2015).
[20] E. Michel, H. Ibach, and C. M. Schneider, Surf. Interface Anal. **48**, 1104 (2016).
[21] E. Michel, H. Ibach, C. M. Schneider, D. L. R. Santos, and A. T. Costa, Phys. Rev. B **94**, 014420 (2016).
[22] H. Ibach, Surf. Sci. **630**, 301 (2014).
[23] S. J. Pickart, H. A. Alperin, V. J. Minkiewicz *et al.*, Phys. Rev. **156**, 623 (1967).
[24] K. Heinz, S. Müller, and L. Hammer, J. Phys.: Condens. Matter **11**, 9437 (1999).
[25] F. Huang, M. T. Kief, G. J. Mankey, and R. F. Willis, Phys. Rev. B **49**, 3962 (1994).
[26] P. Poupoulos and K. Baberschke, J. Phys.: Condens. Matter. **11**, 9495 (1999).
[27] B. Schulz, R. Schwarzwald, and K. Baberschke, Surf. Sci. **307–309**, **Part B**, 1102 (1994).
[28] J. Rajeswari, Thesis, University of Duisburg, 2013.
[29] J. Rajeswari, H. Ibach, and C. M. Schneider, Phys. Rev. B **87**, 235415 (2013).
[30] J. Hong and D. L. Mills, Phys. Rev. B **62**, 5589 (2000).
[31] P. Buczek, A. Ernst, and L. M. Sandratskii, Phys. Rev. B **84**, 174418 (2011).
[32] M. P. Gokhale, A. Ormeci, and D. L. Mills, Phys. Rev. B **46**, 8978 (1992).
[33] O. Hjortstam, J. Trygg, J. M. Wills, B. Johansson, and O. Eriksson, Phys. Rev. B **53**, 9204 (1996).
[34] C. A. F. Vaz, G. Lauhoff, J. A. C. Bland *et al.*, J. Magn. Magn. Mater. **313**, 89 (2007).
[35] A. M. N. Niklasson, B. Johansson, and H. L. Skriver, Phys. Rev. B **59**, 6373 (1999).
[36] H. Ibach, J. Rajeswari, and C. M. Schneider, Rev. Sci. Instrum. **82**, 123904 (2011).
[37] C. M. Schneider, P. Bressler, P. Schuster, J. Kirschner, J. J. deMiguel, and R. Miranda, Phys. Rev. Lett. **64**, 1059 (1990).
[38] J.-H. Moon, S.-M. Seo, K.-J. Lee, K.-W. Kim, J. Ryu, H.-W. Lee, R. D. McMichael, and M. D. Stiles, Phys. Rev. B **88**, 184404 (2013).
[39] A. Crépieux and C. Lacroix, J. Magn. Magn. Mater. **182**, 341 (1998).
[40] A. T. Costa, R. B. Muniz, and D. L. Mills, Phys. Rev. B **68**, 224435 (2003).
[41] L. Bergqvist, A. Taroni, A. Bergman, C. Etz, and O. Eriksson, Phys. Rev. B **87**, 144401 (2013).
[42] A. T. Costa, R. B. Muniz, and D. L. Mills, Phys. Rev. B **70**, 054406 (2004).
[43] A. Clarke, G. Jennings, R. F. Willis *et al.*, Surf. Sci. **187**, 327 (1987).